EarthArXiv Cover Page

Precipitation-induced Geometry Evolution during Reactive Transport: Experimental and Numerical Insights into Stochastic Dynamics of Mineral Growth

Mohammad Nooraiepour [1,*], Mohammad Masoudi and Helge Hellevang

[1] Department of Geosciences, University of Oslo, P.O. Box 1047 Blindern, 0316 Oslo, Norway

* Correspondence: mohammad.nooraiepour@geo.uio.no

This is a non-peer-reviewed preprint submitted to EarthArXiv. The manuscript will be submitted to multidisciplinary open-access journals after further development of this initial work submitted to a conference. The subsequent versions of this manuscript may therefore have different content.

Please feel free to contact the author. Your feedback and comments are welcomed.

Introduction

Crystal nucleation, precipitation, and growth during a reactive fluid flow and solute transport are critical in a vast range of natural and industrial systems. Mineral growth is a prime example where (geo)chemical reactions give rise to geometry evolution in porous media. The precipitation reactions can reduce porosity, alter pore space connectivity and morphology, modify tortuosity, and deteriorate permeability, and therefore, change the fluid flow and solute transport. Additionally, precipitation reshapes the available surface area for growth, leading to changes in the system's reactivity, reaction progress, and reaction rates. The target is to ideally limit the mineral growth in many applications, such as avoiding damage to reservoir permeability and solid precipitation near CO_2 injection wells (Nooraiepour et al., 2018a,b). In other cases, the target is to maximize crystal growth, such as sealing fractured caprocks of sequestration sites or increasing mineral trapping. Modeling this reactive transport process is complicated because it requires coupling flow, transport, and chemical processes that are often characterized by different temporal and spatial scales (Masoudi, 2021).

Mineral reaction rates are traditionally computed using the Transition State Theory (TST) developed approximately four decades ago. The straightforward nature of the TST equation has made it, by far, the most used kinetic model used to predict a range of natural and engineered phenomena. However, using just one equation to predict growth rates from dissolution-rate data ignores and violates the principal assumptions in deriving the TST model. Moreover, the simplification and assumptions of TST lead to unrealistically high precipitation rates, even at low supersaturations. This knowledge led to new kinetic models and formulations based on Classical Nucleation Theory (CNT) and non-equilibrium surface growth models. Because of the complex interactions between reaction processes and transport across time- and length-scales, even when the total amount of secondary precipitates is precisely captured, it is nontrivial to predict the evolution of transport properties (Nooraiepour et al., 2021a,b; Masoudi et al., 2021). The kinetic models fail to predict where crystals will nucleate and form in the pore space, apart from transport properties. It is essential to predict the distribution of the precipitates besides their amount, particularly when clogging is expected.

Nucleation is the pre-growth process that controls the primary position of any mineral precipitation. Mineral nucleation is a probabilistic process where crystals might nucleate anywhere given similar conditions, such as surface properties, supersaturation, and temperature (Hellevang et al., 2019). It is imperative to use a probabilistic approach or an upscaled physically sound representation of nucleation process to predict the effect of precipitation on porous medium hydrodynamics. Motivated by the importance of incorporating stochastic dynamics of nucleation, crystallization, and growth kinetics in studying a variety of multiphase and multiscale processes occurring in geo-environmental and geo-energy systems, this work presents experimental and numerical results delineating geometry evolution induced by mineral precipitation.

Materials and Methods

We chose a natural multi-mineral quartz-rich sandstone as the geomaterial experimental substrate. The Brumunddal sandstone was selected, which shows an average porosity of 18% (15-24%) and permeability of 100 mD (50-200 mD). We cut core samples in disk shape (2.5 cm diameter and 1.5 cm height) to prepare substrates for microfluidic experiments. First, the specimens were washed in deionized water (DI-water) and an ultrasonic bath to clean the substrate surfaces and the porous medium. Subsequently, a series of automatic polishing steps were conducted to provide a flat unscratched surface. Cleaning in the ultrasonic bath was repeated after polishing to remove rock fragments from the surface.

For the calcium carbonate synthesis experiments, we prepared stock solutions from respective crystalline solids (ACS reagent, ≥ 99.8%) of calcium chloride ($CaCl_2$) and sodium bicarbonate ($NaHCO_3$) by adding the well-defined weight of salts to the DI-water (Milli-Q water). We used the PHREEQC v3 for aqueous geochemical calculations to compute solute supersaturation before the experiments. The supersaturation (Ω) is defined as the saturation ratio given by the ion activity product divided by the equilibrium constant. The stoichiometry estimates were based on equilibrium with atmospheric CO_2 pressure. Nine experimental sets were conducted at three supersaturations (Ω = 15, 50, and 130x) and three temperatures (T = 20, 40, and 60°C). The elapsed time (t) for the tests were 6, 48, and 96 hours. Therefore, a total of 27 experiments (3×3×3 sets of Ω-T-t) were carried out. Three polished and cleaned sandstone substrates were placed inside the microfluidic vessel and entirely submerged into the solution. Afterward, the microfluidic vessel was closed, sealed, and placed inside a temperature-controlled air bath to ensure temperature uniformity throughout the experiments. Further details of the laboratory apparatus are given in Fazeli et al. (2020) and Moghadam et al. (2019).

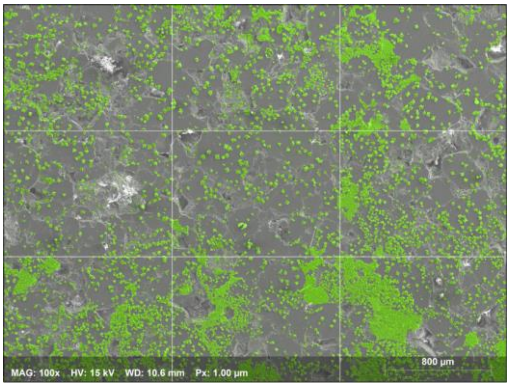

Figure 1 *A surface mosaic map of nine BSE-SEM regions with EDS identification of calcium carbonate crystals (color-coded in green). Magnification = 100x and length-scale = 800 microns.*

Scanning electron microscopy (SEM), backscattered (BSE) and secondary electrons (SE) imaging, was used to study the surface structure and mineral growth. The energy-dispersive x-ray spectroscopy (EDS) was used for chemical analyses and element mapping. Three random locations were selected and analysed for SEM-EDS surface mapping for each substrate. A mosaic map of nine SEM-EDS images covering an approximately 10.5 mm^2 area was acquired with a spatial resolution of 1 µm. For digital image processing, the superimposed calcium phase map (color-coded in green) on the surface mosaic map was selected as an input. Figure 1 shows a typical surface mosaic map comprising nine regions of ordinary BSE SEMs. Further details are given in Nooraiepour et al. (2021a).

Figure 2 presents the semi-automated workflow for digital image processing of surface mosaic maps to identify and quantify precipitated crystals. First, two-dimensional surface maps were filtered with a non-local means filter to remove noise and improve demarcation between phases. Subsequently, contrast enhancement filters were applied (histogram equalization and linear contrast adjustment). Based on the histogram of grey values (two distinct distributions), the mosaic maps were segmented and converted into binary images (Fig. 2b). The inverted (mask) transformation of the binary map was analyzed in the ImageJ/Fiji open-access image processing package to identify, outline, and quantify the precipitated calcium carbonate crystals (Figs. 2d-e). Finally, we computed Shannon Entropy for each mosaic map to quantify randomness and spatial disorder within the system.

For numerical simulations, we used the Lattice Boltzmann Method (LBM) to solve the advection-diffusion-reaction equation for tracking the concentration of different species. We developed a reactive transport model based on our recently proposed probabilistic nucleation and crystal growth theory (Nooraiepour et al., 2021b). The D2Q9 lattice scheme was used in a 400×400 µm simulation domain representing a homogeneous nonreactive substrate to model the surface nucleation and growth. The periodic boundary condition is applied for all the boundaries. An infinite source of a solution on top of the substrate was imposed. The first step in the LBM simulations is probabilistic nucleation, which is the necessary condition for growth or for the reaction to start $\{A_{(aq)} \rightleftarrows A_{(s)}\}$ (cf. Masoudi et al. 2021, Nooraiepour et al., 2021b).

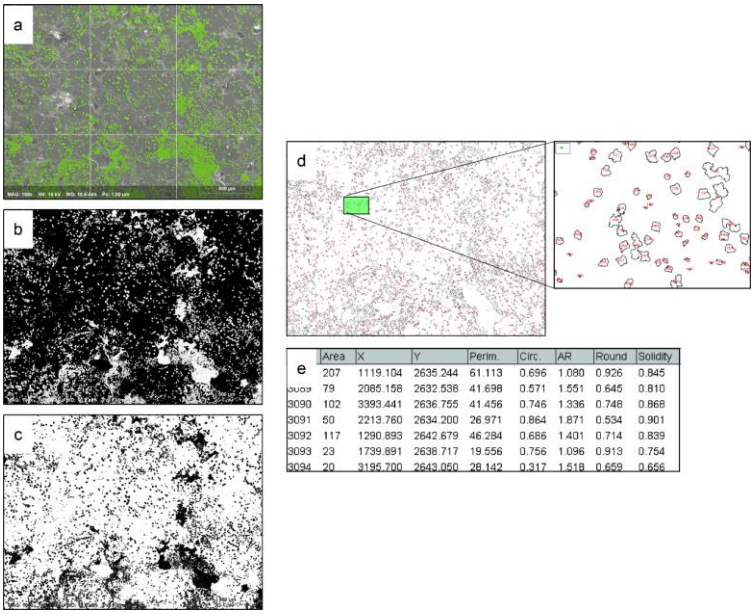

Figure 2 *Semi-automated workflow for digital image processing of surface mosaic maps to identify and quantify precipitated calcium carbonate crystals on top of the multi-mineral sandstone substrate. (a) SEM-EDS surface map; (b) Binary conversion of "a" after noise removal, contrast enhancement, and thresholding of grayscale histogram; (c) Inverted transformation of binary map; (d) Identification and quantitation of crystals; Properties of single crystals or crystal batches were quantified via the exact linear scale of mosaic maps and length-pixel ratio; (e) An exemplary table indicating properties of crystals quantified in our analysis.*

Results and Discussion

Classical nucleation theory indicates that supersaturation, temperature, and interfacial free energy are the main factors determining the number and distribution of stable growing crystals. The image processing results of 27 experiments (3×3×3 sets of Ω-T-t) are presented in Figure 3, where total coverage area (%) and crystal count are plotted versus elapsed time. It also shows the computed entropy of each mosaic map in the second ordinate (y-axis) to measure randomness within the system. With the increase of supersaturation, moving from top to bottom in Figure 3, the distinction between the data points representing different t and T becomes more visible. The coverage area and crystal counts increased remarkably for higher Ω values, particularly for Ω = 130. The increase in the coverage area and crystal counts for a given Ω are subtle for T = 20°C compared to elevated Ts. At Ω = 15, the number of new crystals after initial sampling (t = 6 h) shows a limited increase for the rest of the experiments (t = 48 and 96 hors). Our results suggest temperature has a significant effect on nucleation (compared to supersaturation), and as nucleation is probabilistic, the variability driven by the temperature changes is more pronounced.

In lower supersaturations, the probability of nucleation is lower. As a result, fewer numbers of stable nuclei form at an early time. These stable nuclei consume the available solute in the solution to grow, decreasing the probability of new nucleation events. Thus, low to moderate supersaturations bring about more connected and more extensive solid accumulations. However, when the saturation ratio is too high (for example, Ω = 130), the driving force for growth and nucleation is significant, and scattered patterns might also form. In other words, the low Ω case is associated with the

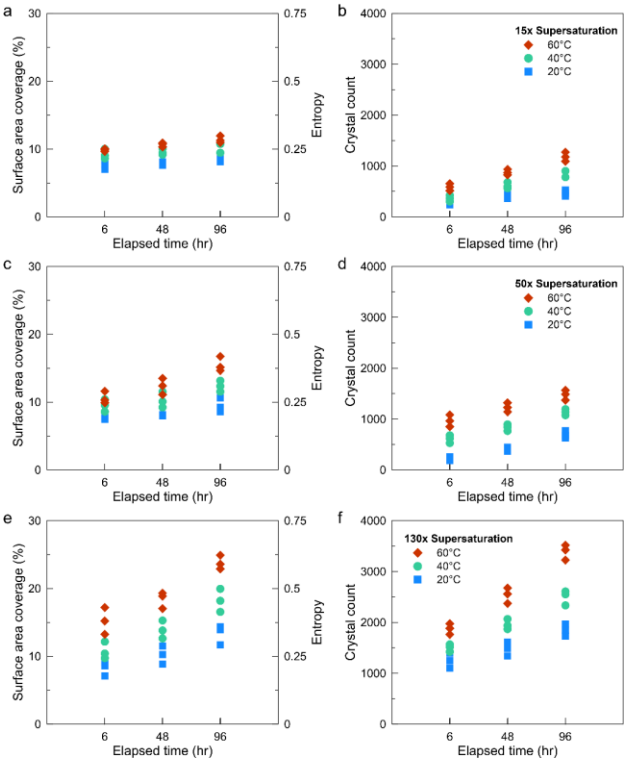

Figure 3 *Total surface area coverage (%), computed Shannon entropy, and the number of the precipitated crystals. (top) 15x, (middle) 50x, and (bottom) 130x supersaturation experiments as a function of elapsed*

limited solute concentration within the stock solution, limiting the number of new nucleation events, therefore less support of the continued growth of previously precipitated solids at early times. At higher supersaturations (Ω = 50 and 130), enough solute is present in the solution to support crystals continued nucleation and growth.

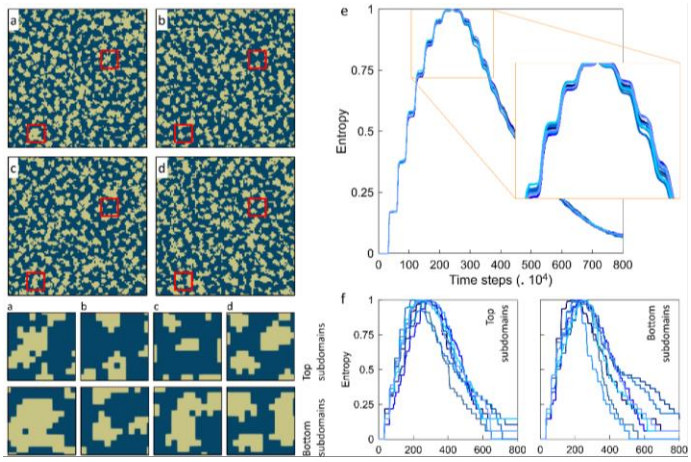

Figure 4 *(left, a-d) Four realizations of a given surface precipitation simulation indicating stochastic amount and distribution of crystals. The red squares show two random subdomains. The subdomains are enlarged for better*

As indicated in Figure 3, when the number of precipitated crystals and areal coverage increases, entropy quantifying randomness and disorder shows an increase. At the beginning of experiments, an ordered system exists where no crystal is present on the surface. The entropy (E) then increases until it reaches a maximum value, approaching one for an entirely random system. We expect the measure of randomness to decline afterward when crystals start covering more and more surface area, and the entropy eventually reaches a constant minimum value if the substrate is fully covered. The larger computed entropy reflects higher disorder within the system, which is the available substrate for crystal nucleation and growth.

In the reactive LBM simulations, the randomness of the spatial distribution of crystals is ensured where we introduced a probabilistic approach for the location and number of nuclei. The growth on the primary and the secondary substrates is a function of the nucleation events. Figure 4 represents four realizations for a simulation scenario with nucleation rate (R_N) = 10^{-2} and reaction rate constant (R_G) = 10^{-6} at 0.85 entropy level (after 1.8×10^6 time steps) to compare the randomness of precipitation distributions. As it is shown in Figure 4e, the overall evolution described by the entropy for all the realizations is similar. Although, the pattern of surface precipitations, crystal locations, and their amount vary. The difference in realizations is more evident if we consider smaller subdomains (red squares) in each realization.

Within the two subdomains, precipitation amounts, locations, and growth patterns are distinctively different (Fig. 4). Moreover, the probabilistic control on nucleation and growth is better discernible within the two subdomains compared to original domains. To quantify the spatial randomness of distributions, we computed entropy for each subdomain in Figure 4f. The degree of scatter and dissimilarity in evolution paths is notably higher, particularly for plots of bottom subdomain. At similar evolution time (at 1.8×10^6 time steps), the original realizations showed a 0.85 entropy level while the disorder in subdomains varies from 0.65 to 0.95. It indicates that the size of the spatial and temporal resolutions govern the randomness of the spatial distributions.

Conclusions

The present study focuses on surface mineral nucleation, precipitation, and growth. We delineate nucleation as the first step in the precipitation and growth chain of events. The results indicated the probabilistic nature of the process, which is affected by the physiochemistry of the aqueous phase and governed by fluid-solid surface interactions. The research outcomes highlighted that it is crucial to consider surface properties, preferential locations, and nucleation and growth on the previously precipitated crystal (secondary substrate). We underscore the importance of theoretical reactive transport models considering the probabilistic nature of nucleation events before crystal formation.

Acknowledgements

The authors thank the "solid and salt precipitation kinetics during CO_2 injection into reservoir" project, (EEA & Norway Grants, UMO-2019/34/H/ST10/00564, Grieg program) for supporting the research. The HPC simulations was performed on the Norwegian Research and Education Cloud (NREC). MN acknowledges the Faculty of Mathematics and Natural Sciences, University of Oslo for the Kristine Bonnevie scholarship.

References

Fazeli, H., Nooraiepour, M., and Hellevang, H. [2020]. Microfluidic study of fracture dissolution in carbonate-rich caprocks subjected to CO_2-charged brine. ACS I&EC Research, 59(1).

Hellevang, H., Wolff-Boenisch, D., and Nooraiepour, M. [2019]. Kinetic control on the distribution of secondary precipitates during CO_2-basalt interactions. E3S Web of Conferences, 98.

Masoudi, M., Fazeli, H., Miri, R., and Hellevang, H. [2021]. Pore scale modeling and evaluation of clogging behavior of salt crystal aggregates in CO_2-rich phase during carbon storage. International Journal of Greenhouse Gas Control, 111, 103475.

Masoudi, M. [2021]. Near wellbore processes during carbon capture, utilization, and storage (CCUS): an integrated modeling approach. Doctoral thesis, University of Oslo, pp. 206.

Moghadam, J.N., Nooraiepour, M., Hellevang, H., Mondol, N. H., and Aagaard, P. [2019]. Relative permeability and residual gaseous CO_2 saturation in the Jurassic Brentskardhaugen Bed sandstones, Wilhelmøya, western central Spitsbergen, Svalbard. Norwegian Journal of Geology, 99(2), 1–12.

Nooraiepour, M., Fazeli, H., Miri, R., and Hellevang, H. [2018a]. Effect of CO_2 phase states and flow rate on salt precipitation in shale caprocks - A microfluidic study. ACS ES&T, 52(10).

Nooraiepour, M., Fazeli, H., Miri, R., and Hellevang, H. [2018b]. Salt precipitation during injection of CO_2 into saline aquifers: lab-on-chip experiments on glass and geomaterial microfluidic specimens. 14th Greenhouse Gas Control Technologies Conference (GHGT-14), Melbourne, 21-26 October 2018.

Nooraiepour, M., Masoudi, M., Shokri, N., and Hellevang, H. [2021a]. Probabilistic nucleation and crystal growth in porous medium: New insights from calcium carbonate precipitation on primary and secondary substrates. ACS Omega, 6(42), 28072–28083.

Nooraiepour, M., Masoudi, M., and Hellevang, H. [2021b]. Probabilistic nucleation governs time, amount, and location of mineral precipitation and geometry evolution in the porous medium. Scientific Reports 11.